Optical properties of highly n-doped germanium obtained by in-situ doping and laser annealing

J. Frigerio[1*], A. Ballabio[1], K. Gallacher[2], V. Giliberti[3], L. Baldassarre[3], R. Millar[2], R. Milazzo[4], L. Maiolo[5], A. Minotti[5], F. Bottegoni[6], P. Biagioni[6], D. Paul[2], M. Ortolani[3], A. Pecora[5], E. Napolitani[4] and G. Isella[1]

[1] L-NESS, Dipartimento di Fisica, Politecnico di Milano,Polo di Como, Via Anzani 42, I-22100 Como, Italy
[2] School of Engineering, University of Glasgow, Rankine Building,Oakfield Avenue, Glasgow G12 8LT, United Kingdom
[3] Dipartimento di Fisica, Sapienza Università di Roma, Piazzale Aldo Moro 5, I-00185 Rome, Italy
[4] Dipartimento di Fisica e Astronomia, Università di Padova and CNR-IMM Matis, Via Marzolo 8, I-35131 Padova, Italy
[5] CNR-IMM, Via del Fosso del Cavaliere 100, 00133 Roma, Italy
6 Dipartimento di Fisica, Politecnico di Milano, piazza Leonardo da Vinci 32, I-20133 Milano, Italy

*jacopo.frigerio@polimi.it

Abstract

High n-type doping in germanium is essential for many electronic and optoelectronic applications especially for high performance Ohmic contacts, lasing and mid-infrared plasmonics. We report on the combination of in-situ doping and excimer laser annealing to improve the activation of phosphorous in germanium. An activated n-doping concentration of $8.8x10^{19}$ cm^{-3} has been achieved starting from an incorporated phosphorous concentration of $1.1x10^{20}$ cm^{-3}. Infrared reflectivity data fitted with a multi-layer Drude model indicate good uniformity over a 350 nm thick layer. Photoluminescence demonstrates clear bandgap narrowing and an increased ratio of direct to indirect bandgap emission confirming the high doping densities achieved.

I Introduction

Heavily doped n-type germanium is attracting an increasing interest driven by its potential applications in microelectronics, photonics and mid-infrared (mid-IR) plasmonics. Ge based CMOS [1] is under investigation for end-of-the-roadmap electronic applications, where low resistivity n-type Ohmic contacts [2] and good n^+-p junctions [3] are mandatory in order to take full advantage of the superior electron mobility of Ge as compared to Si. Doping [4,5] is the key tool, together with tensile strain [6-8], to engineer the band structure of germanium for the development of an efficient Ge-on-Si laser. Moreover Ge has been identified as a key-material for the realization of mid-IR waveguides [9,10] due to the absence of strong intraband transitions in the 1.9-14 μm wavelength range. Recently it has been demonstrated that, by doping germanium in the low 10^{19} cm^{-3} range, it is possible to tune its plasma wavelength to around 10 μm (plasma frequency $\omega_p \approx 1000$ cm^{-1}) [11] thus enabling mid-IR plasmon enhanced sensing [12-13]. In addition, the compatibility of germanium with standard silicon foundry processes can boost the pervasive exploitation of plasmonic effects in the infrared.

In order to fully exploit the potential of Ge-on-Si plasmonics, however, a doping density approaching 10^{20} cm^{-3} over a uniform doping profile of the order of a few electromagnetic skin depths, i.e. approximately 300-500 nm, would be desirable in order to cover the whole relevant fingerprint region in the mid-infrared. Achieving a uniform activation profile is extremely relevant for mid-IR sensing since layers with different electron concentrations would lead to a variation of the plasma frequency within the Ge layer and a consequent smearing-out of all resonant effects. Furthermore, the thickness of such highly-doped layer should be sufficient to clearly determine the plasma frequency ω_p separating the frequency region ($\omega > \omega_p$) where the semiconductor is highly transparent, from the frequency region ($\omega < \omega_p$) where a metallic behavior is observed. Phosphorous doping of Ge-on-Si epilayers performed at temperatures around T≈500-600 °C and employing GeH_4 and PH_3 as precursor gases typically results in an activated doping density $n_e \approx 2\times10^{19}$ cm^{-3} [14,15]. Deposition at lower temperatures, which requires the use of specialized precursor gases, resulted in an increased activation ($n_e \approx 6\text{-}7\times10^{19}$ cm^{-3}) [16-18] even though a much higher dopant atom incorporation of N_D≈1-$2\times10^{20}cm^{-3}$ was observed in these cases. Electron densities as high as $n_e \approx 2.2\times10^{20}$ cm^{-3} have been obtained by in-situ doping, although on layers of thickness below 100 nm, by using a combination of molecular beam epitaxy (MBE) for Ge deposition and low temperature exposure to PH_3, which leads to the formation of a mono-atomic P layers, subsequently incorporated [19] by means of Ge regrowth and thermal treatments. The implementation of such atomic-layer doping approach in a CVD reactor has been only partially successful, possibly because of the critical role played by hydrogen adsorbed on the Ge surface during PH_3 exposure. A combination of P-implantation and flash-lamp-annealing has also been used to achieve an active carrier concentration of $n_e \approx 2.2\times10^{20}$ cm^{-3} however the implantation depth limits the thickness of the doped layer to approximately 150nm [20]. An alternative approach to increase the active doping concentration is laser thermal annealing (LTA). In the LTA process one or more laser pulses are used to melt the ion-implanted or in-situ doped semiconductor. The subsequent fast, out of equilibrium recrystallization process, enhances the substitutional incorporation of dopants in the material. Moreover, by using pulses in the nanoseconds range, dopant diffusion is inhibited and a box-like doping profile can be obtained. LTA has been successfully employed to achieve a doping activation above 10^{20} cm^{-3} in implanted bulk [21,22] Ge and in in-situ doped Ge-on-Si epilayers [23]. In both cases, however, only electrical measurements have been performed to characterize the highly doped region, which is limited to a thickness of ~ 100 nm. In this work we have investigated the use of LTA to obtain uniform active doping levels close to 10^{20} cm^{-3} in 500 nm thick, in-situ doped Ge-on-Si. The structural properties of the samples have been investigated by atomic force microscopy (AFM), secondary ion mass spectrometry (SIMS) and μ-Raman spectroscopy and the optical properties have been explored, in the mid-IR, by means

of infrared reflectometry and, in the near-IR, by means of photoluminescence spectroscopy. The measured plasma frequency of $\omega_p \approx 1850$ cm^{-1} makes these epilayers suitable for plasmon-enhanced sensing of most organic substances, as the important carbonyl-carboxyl fingerprint region at 1600-1750 cm^{-1} is now fully covered if compared to previous doped semiconductor plasmonic devices [12-24]. On a different perspective, band gap narrowing (BGN) and the residual tensile strain of ≈ 0.38%, induced by LTA are seen to red-shift the direct bandgap PL to ≈ 1.8 μm making this doping procedure attractive for integrated photonics applications [25,26].

II Methods

The sample was grown by Low-Energy Plasma-Enhanced Chemical Vapor Deposition (LEPECVD) [27] and it consists of a ≈ 500 nm thick Ge layer deposited at 500 °C at a rate of 1 nm/s with a GeH_4 flux of 20 sccm. The doping was obtained by adding 0.35 sccm of PH_3 during the growth. The structural properties of the as grown sample were measured by atomic force microscopy (AFM) and by high-resolution x-ray diffraction (HR-XRD) reciprocal space mapping (RSM) about the (004) and (224) (grazing incidence) reflections using a PANalytical X'Pert PRO MRD diffractometer. Out-of-plane and in-plane lattice parameters, as well as the strain state were measured (relative to the Si reflection) for the Ge peak. LTA was performed in vacuum by using a Lambda Physik LPX 305 XeCl excimer laser (λ=308 nm, 28 ns pulse duration) with an energy density of 1 J/cm^2. The laser annealed area is approximately 100x100 μm^2 covering a sample area of 5×5 mm^2 in total by raster scanning the sample with 1 mm steps and firing a total of 25 laser shots. The incorporated doping profile has been measured by SIMS using a CAMECA ims-4f mass spectrometer. An O_2^+ ion beam with an accelerating voltage of 3 keV, rastered over a 250×250 μm^2 area, was used for sputtering, while collecting $^{31}P^{16}O^+$ secondary ions. The calibration of the P concentration was performed by measuring a Ge standard with known P areal density with an accuracy of ±15%. The measurement reproducibility is ±5%. The active doping profile has been extracted from the frequency-dependent reflectivity of the samples by applying a fitting procedure. The frequency-dependent absolute normal-incidence reflectivity was measured in the 600-6000 cm^{-1} (1.6–17 μm wavelength) range with an infrared microscope (Bruker Hyperion) and a nitrogen-cooled photovoltaic detector (Infrared Associates HgCdTe) coupled to a Bruker IFS 66v Fourier-Transform spectrometer (FTIR). The knife-edge aperture of the microscope was kept at 100×100 μm^2 while scanning the 5×5 mm^2 area subject to LTA hence obtaining an active-carrier concentration map. The reflectivity spectrum measured at the locations in the center of different LTA spots was approximately the same.

The plasma frequencies ω_P of the samples has been obtained by fitting the experimental reflectivity with a multi-layer Drude model. Each physical layer is modeled via standard Drude model as an independent layer and the reflectivity at the interfaces is taken into account through the Fresnel coefficients [11]. Once the plasma frequencies are obtained, the active carrier concentration of each layer can be calculated by using equation 1:

$$n_e = \frac{\omega_p^2 m^*}{\varepsilon_0 e^2} \quad (1)$$

The extraction of n_e from IR data only relies on the knowledge of the effective mass $m^* \approx 0.12 m_e$ (where m_e is the free electron mass) and the IR low-frequency dielectric constant of Ge $\varepsilon_\infty \approx 16$, which are known with a much higher accuracy than the Hall factor, the specific Ohmic contact resistivity or the thickness of the heavily doped layer, all affecting the analysis of electrical measurements [16]. Micro-Raman measurements are taken using a confocal microscope (Witec Alpha RAS), using a 532 nm excitation source and a 100 X 0.9 NA objective. The spectrometer is calibrated using a mercury lamp prior to measurement. The 532 nm pump is absorbed within 20 nm of the Ge layer and therefore the measurement only probes the strain at the top plane of the epilayer. Once focused on the sample surface, the pump power intensity is reduced until heating is eliminated from the measurement. Long integration times (> 5s) are typically used to allow for low power densities. The resultant spectra are baseline corrected, and fitted with a psuedo-Voigt function (Gaussian Lorentzian sum) in order to determine the peak position. PL spectra have been acquired at room temperature by using a Bruker Vertex 70 FTIR system. The samples were optically pumped with a continuous wave frequency doubled Nd:YAG laser operating at 532 nm wavelength. The laser illuminates the sample through an aperture in a parabolic mirror. The sample emission is collected by this mirror, which then couples the emission into the internal Michelson interferometer of the FTIR system before detection by an extended InGaAs camera [28]. In order to discriminate against ambient black-body radiation, a reference measurement is taken immediately before the PL measurement. This spectrum shows a black-body tail towards the 2.5 μm cut-off of the InGaAs detector, and is subsequently subtracted from all PL spectra.

III Structural characterization

The epitaxial structure of the as grown sample has been characterized by high-resolution X-Ray diffraction to check the crystalline quality of the sample and to measure the in-plane strain $\varepsilon_{\parallel}$. The reciprocal space maps about the (004) and (224) Si reflections are reported in figure 1 a and b respectively.

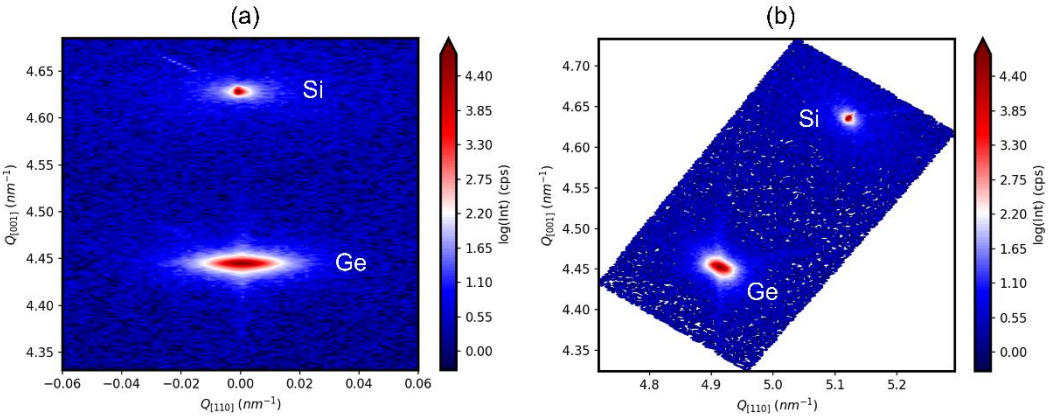

Figure 1: Reciprocal space maps about the (004) and (224) Si Reflections of the as grown sample

Out-of-plane and in-plane lattice parameters, were measured for the Ge peak and an in-plane strain of $\varepsilon_{\parallel} \approx 5 \times 10^{-4}$ was then obtained using the known lattice parameter and the elastic constants of relaxed Ge. Ge-on-Si typically exhibits a residual tensile strain, induced by the thermal expansion coefficient mismatch between Ge and Si developing during cool-down from the growth (or annealing) temperature to room-temperature, consistently with the relatively low deposition temperature employed in our work, a negligible tensile strain is found in the as-grown sample. Strain effects related to the dopant atoms incorporation are negligible in the case of phosphorous [29] and can therefore be neglected. The small dimensions of the laser annealed area did not allow a reliable HR-XRD characterization of the laser annealed sample, therefore the µ-Raman set-up was used to compare the as-grown and annealed areas. A comparison of the two Raman spectra is shown in figure 2. An in-plane strain of $\varepsilon_{\parallel} \approx 3.7 \times 10^{-3}$ for the annealed sample has been deduced from the experimentally measured Raman shift by using equation 2:

$$\Delta\omega = \frac{\varepsilon_{||}}{\omega_0}\left[q - p\frac{C_{12}}{C_{11}}\right] \qquad (2)$$

Where $\Delta\omega$ is the Raman shift (see fig. 2), ω_0 is the wavenumber of the peak of the as grown sample, p and q are the Raman deformation potentials [30] and C_{11} and C_{12} are the elastic constants of Ge.

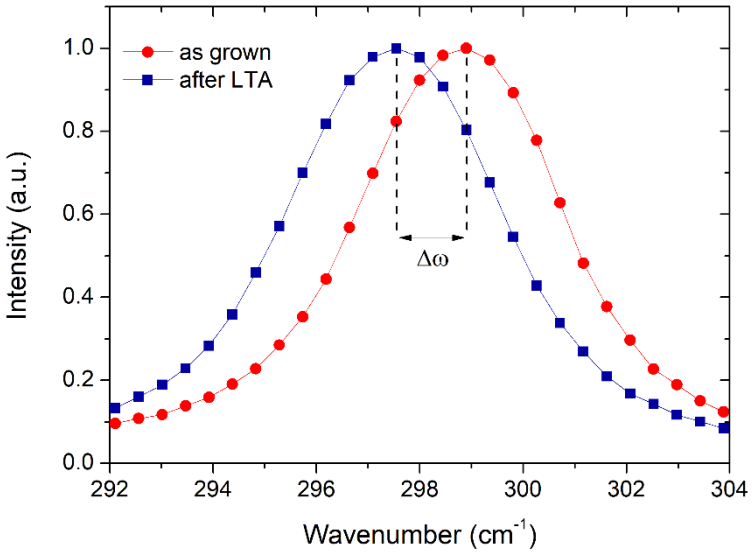

Figure 2: Raman spectra of the as grown sample (red circles) and after the LTA (blue squares). Δω is the experimentally measured Raman shift.

Tensile strain is not observed in laser annealed bulk Ge [31] while it has already been reported in Ge-on-Si epilayers [23]: this suggests that, also in the case of laser annealed epilayers, tensile strains develops due to the thermal expansion coefficient mismatch between Ge and Si. It is worth noticing that the measured strain exceeds the maximum tensile strain $\varepsilon_{\parallel} \approx 2.8 \times 10^{-3}$ achievable for the case of Ge-on-Si heterostructure cooling down from the Ge melting temperature (T_H = 937°C) to room temperature [32]. Such limiting value of $\varepsilon_{\parallel} \approx 2.8 \times 10^{-3}$ is obtained only in the case that both epilayer and substrate cool down from the same initial temperature T_H. If we allow the substrate to reach a maximum temperature lower than T_H, as is the case for the highly non-uniform temperature distribution attained by laser annealing, strain values larger than 2.8×10^{-3} are indeed achievable. Two 20×20 μm^2 atomic force microscopy (AFM) scans of the Ge-on-Si sample before and after the LTA are reported in figure 3 a and b respectively. The as-grown sample features a smooth surface with an RMS roughness of about 0.5 nm.

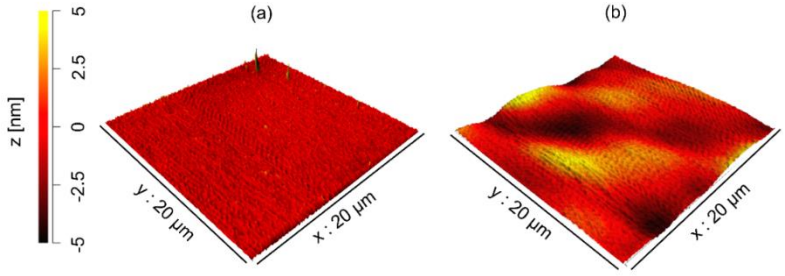

Figure 3: 20×20 μm^2 AFM scans of the sample before (a) and after (b) the LTA process.

After LTA, the AFM scan reveals surface undulations due to re-crystallization. These undulations have a periodicity of ≈10 µm and an average vertical amplitude of about 5 nm. The effects of laser annealing on the P incorporation profile are shown in figure 4. The incorporated dopant concentration in the as-grown sample has an almost constant value of about 1.1×10^{20} cm^{-3} over 450 nm. Such P incorporation is almost ten times higher than the one obtained in thermal CVD for similar growth temperatures and PH_3/GeH_4 ratios [17] pointing out the key-role played by the plasma-enhanced deposition. Moreover, by comparing the SIMS profiles before and after irradiation with a 1 J/cm^2 pulse, it can be noticed that only a very slight redistribution of dopants takes place, in agreement with the absence of redistribution expected from Fick's law in the case of zero concentration gradient and with reflecting boundary conditions at the surface (i.e. no P surface segregation or out-diffusion).

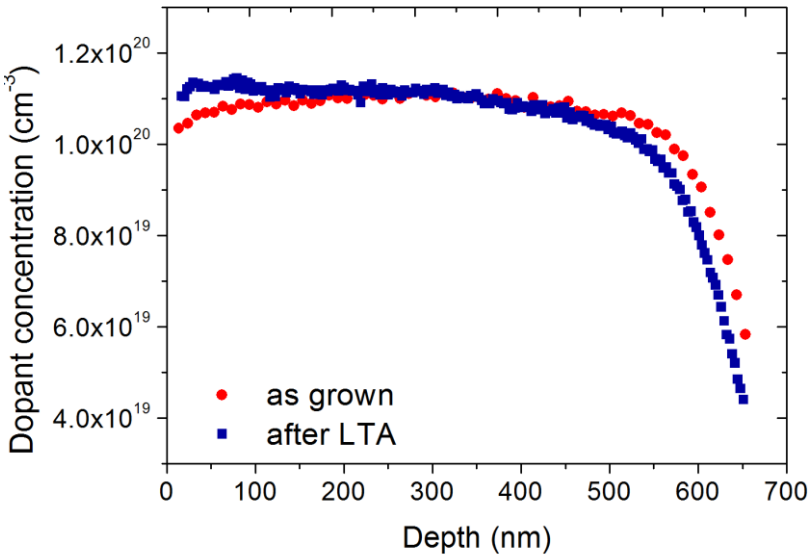

Figure 4: The SIMS profiles of the sample before (red circles) and after (blue squares) the LTA process.

IV Optical characterization

The reflectivity spectra of the sample before and after the LTA process are reported in figure 5.

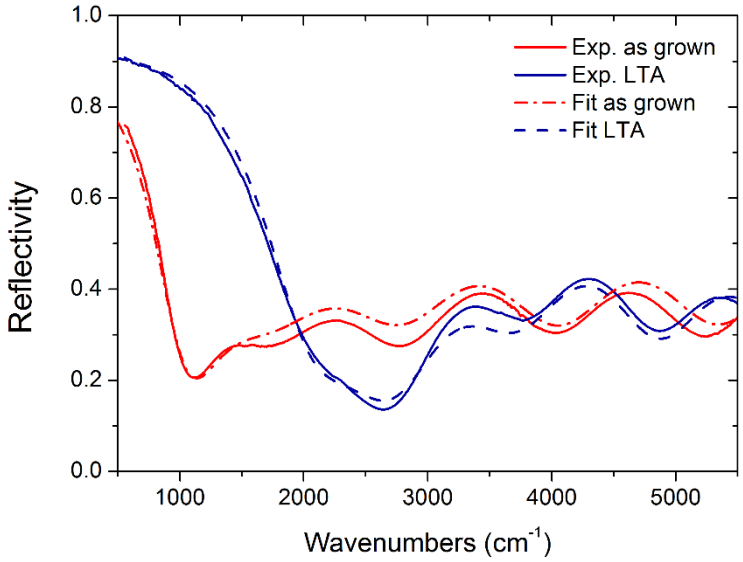

Figure 5: The reflectivity spectra of the as grown sample (red line) and of the LTA treated sample (blue line). The multi-layer Drude fitting of both spectra are reported as a red dashed line and as a dash-dotted blue line respectively.

The as-grown sample has been fitted with an homogeneous dielectric function throughout the Ge thickness of 500 nm. A plasma frequency $\omega_P \cong 970$ cm^{-1} has been retrieved, which corresponds to an active carrier concentration $n_e \cong 2.1\pm0.2 \times 10^{19}$ cm^{-3}. At least two different Ge layers (350 nm and 150 nm thick) had to be used instead to reproduce the reflectivity of the sample subject to LTA. The plasma frequencies retrieved from the fitting are approximately located at $\omega_P \cong 1850$ cm^{-1} for the top layer and 1159 cm^{-1} for the bottom layer. The carrier concentrations calculated with equation 1 are $n_e \cong 8.8 \pm 0.9 \times 10^{19}$ cm^{-3} and $n_e \cong 3.1 \pm 1 \times 10^{19}$ cm^{-3} respectively. This result suggests that the bottom part of the Ge film did not experience melting and recrystallization as the top part. We stress that the double-layer Drude fit does not indicate in this case the presence of a physical interface at a depth of 350 nm, rather it provides an average description of the doping profile in the Ge thickness. The use of more layers or of a doping-dependent profile would probably provide a more accurate description, at the expense of the simplicity of the model. The high activation achieved using LTA is confirmed by photoluminescence (PL) measurements.

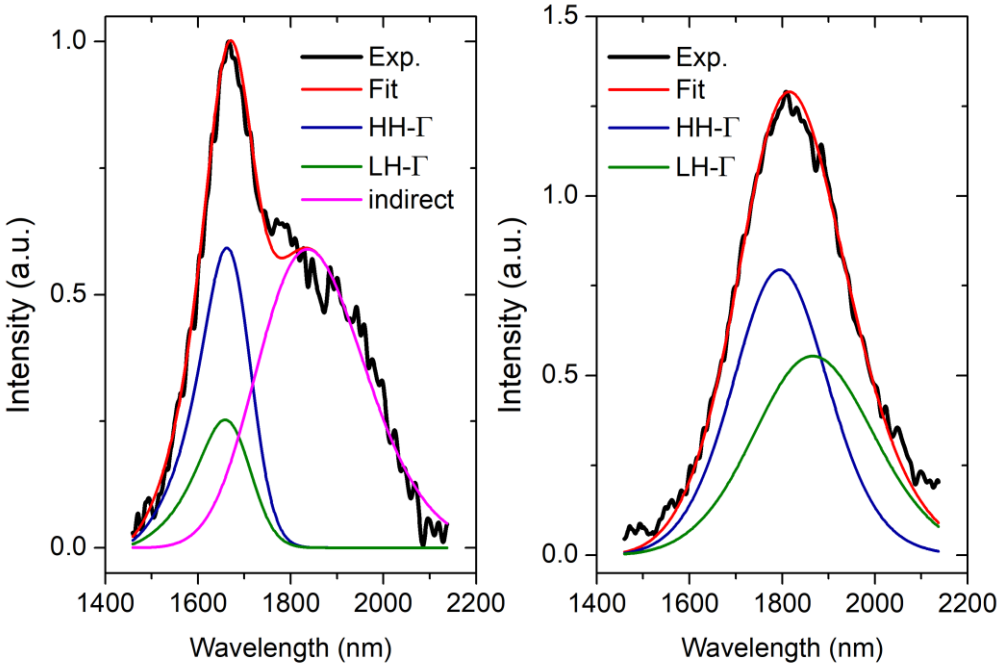

Figure 6: PL intensity (normalized at the intensity of the direct-gap related peak of the as grown sample) as a function of the wavelength from an as-grown region of the Ge-on-Si epilayer (a), and of the LTA treated region (b). The PL lineshape has been analyzed considering the recombination from Γ-heavy holes (blue line), Γ-light holes (green line) and indirect radiative transitions (magenta lines).

The PL spectrum of the as grown epilayer (see figure 6a) is dominated by a sharp peak at $\lambda \approx 1.67$ µm, which can be attributed to direct-gap recombination. As typically observed in Ge-on-Si epilayers the indirect related PL (the shoulder extending in the range ≈ 1.8 – 2.1 µm) is relatively weak due to the inherently low radiative recombination rate of phonon-assisted transitions and the stronger impact of non-radiative recombination on L-valley electrons, as compared to Γ-valley electrons [33]. The broadening of the indirect-gap peak [34] is consistent with the relatively high doping level measured by IR reflectometry ($n_e = 2.1\times10^{19}$ cm^{-3}) for this sample, which corresponds to a Fermi level located ~0.03 eV above the L-valley minima. The indirect related PL was modeled with a Gaussian profile (magenta line in Fig. 6a) with a FWHM of ~0.18 eV and subtracted from the PL spectra to better analyze the direct-gap related lineshape. Camacho et al. [35] have proposed a linear phenomenological expression for the estimation of the active carrier density from the peak position of the direct-gap PL, however, it must be noticed that such expression contains a constant term, accounting for the strain-induced BGN, which limits its applicability to Ge-on-Si epilayers with a residual strain comparable to that reported by Camacho et al. ($\varepsilon_{\parallel}\approx2.5\times10^{-3}$). For this reason the direct-gap PL spectra have been fitted with a generalized van Roosbroeck–Shockley expression following the procedure reported in [36,37] and including the strain-induced BGN and related

removal of the HH-LH degeneracy. In this way the contribution to BGN solely due to doping effects can be estimated. As explained in section III, the as-grown sample features a negligible strain $\varepsilon \approx 5\times10^{-4}$, yet strain effects have been included in our modelling with the aim of applying an equal fitting procedure to as-grown and laser annealed samples. The energy of the direct bandgap between the Γ-valley and HH states obtained from the PL data fitting is $E^{d}_{HH} \approx 0.75$ eV. This is in good agreement with the value calculated considering a bandgap narrowing given by the expression $\Delta E_{BGN} = 8.33 \times 10^{-3}\sqrt{n_e/10^{18}}$ (eV), which describes doping-induced effects at the direct and indirect bandgap of Ge [36]. After laser annealing (Fig. 6b) the direct bandgap PL peak is observed to shift to longer wavelengths while the indirect bandgap contribution to the spectra is strongly reduced. This is consistent with the increased population of the Γ valley which strongly effects the relative intensities between direct and indirect transitions [33]. In this case, therefore, the lineshape analysis was performed considering direct bandgap transitions only and a tensile strain $\varepsilon \approx 3.7\times10^{-3}$. In the case of Fig. 5b, the direct bandgaps obtained from the PL data fitting are E^{d}_{HH} (E^{d}_{LH})≈0.69 (0.66) eV. By using the deformation potential and unstrained bandgaps reported in Table I, the strain contribution to the bandgap reduction has been calculated to isolate the BGN contribution and eventually estimate the active carrier density. An active carrier density $n_e \approx 8.9 \times 10^{19}$ cm^{-3} has been obtained after laser annealing, in good agreement with IR reflectometry results. At such doping and strain levels, the Fermi level lays ≈15 meV below the Γ-valley and the relative population ratio between the Γ and L valley electrons is ~3×10^{-3} i.e. an order of magnitude higher than the one expected in the as-grown epilayer.

a^{Γ} (eV)	a^{L} (eV)	b (eV)	E_g^{Γ} (eV)	E_g^{L} (eV)
-9.47	-3.6	-1.88	0.80	0.66

Table I: The direct bandgap hydrostatic deformation potential (a^{Γ}) from Ref [38], indirect bandgap hydrostatic deformation potential (a^{L}) from Ref. [39] and valence band uniaxial deformation potential (b) from Ref. [40]. E_g^{Γ} and E_g^{L} are the unstrained direct and indirect bandgap, respectively.

V Conclusions

In conclusion, we have investigated the capability of the combined use of excimer laser annealing and in-situ doping to achieve high doping levels in Ge-on-Si epilayers. An active doping level of 8.8×10^{19} cm^{-3} fairly constant over a thickness of 350 nm has been measured by infrared

spectroscopy. The absolute reflectance spectra of the LTA treated sample shows a clear transition between the frequency region where the semiconductor is transparent, from the frequency region where a metallic behavior is observed, with a plasma frequency approximately located at 1850 cm^{-1} (∼5.4 μm wavelength). This result paves the way for the realization of Ge-on-Si based plasmon-enhanced sensors covering the whole carbonyl-carboxyl fingerprint region. Moreover, PL spectra confirm the high doping densities achieved in these samples. The significant increase of the relative population ratio between the Γ and L valleys suggest the relevance of such epilayers for the realization of efficient Ge-on-Si laser sources.

Acknowledgments

The research leading to these results has received funding from the European Union's Seventh Framework Programme under grant agreement no. 613055. The authors would like to thank J. Menéndez for his support in PL data analysis.

Bibliography

[1] Pillarisetty R, Nature **479**, 324 (2011).

[2] Gallacher K, Velha P, Paul D J, MacLaren I, Myronov M and Leadley D R, Appl. Phys. Lett. **100** (2) 022113 (2012).

[3] Jamil M, Mantey J, Onyegam E U, Carpenter G D, Tutuc E and Banerjee S K, IEEE Elec. Dev. Lett. **32** (9), 1203 (2011).

[4] Liu J, Sun X, Camacho-Aguilera R , Kimerlingh L C and Michel J, Opt. Lett. **35**, 679-681 (2010)

[5] Camacho-Aguilera R, Cai Y, Patel N, Bessette J T, Romagnoli M, Kimerlingh L C and Michel J, Opt. Expr. **20**, 11316-11320 (2012)

[6] Suess M J, Geiger R, Minamisawa R, Schiefler G, Frigerio J, Chrastina D, Isella G, Spolenak R, Faist J and Sigg H, Nat. Photon. **6**, 466-472 (2013)

[7] G. Capellini et al, J. Appl. Phys. 113 013513 (2013).

[8] R W Millar, Gallacher K, Frigerio J, Ballabio A, Bashir A, MacLaren I, Isella G and Paul D J, Opt. Expr. **24** 4365-4374 (2016)

[9] R. Soref, Nat. Photonics **4**, 495 (2010).

[10] Chang Y C, Paeder V, Hvozdara L, Hartmann J M, and Herzig H P, Opt. Lett. **37**, 2883 (2012).

[11] Frigerio J et al, Phys. Rev. B **94**, 085202 (2016)

[12] Baldassarre L, Sakat E, Frigerio J, Samarelli A, Gallacher K, Calandrini E, Isella G, Paul D J, Ortolani M, and Biagioni P, Nano Lett. **15**, 7225 (2015).

[13] Biagioni P et al, J. Nanophoton. **9**, 093789 (2015)

[14] Cai Y, Camacho-Aguilera R, Bessette J T, Kimerling L C, and Michel J, J. Appl. Phys. **112**, 034509 (2012).

[15] Carroll L, Friedli P, Neuenschwander S, Sigg H, Cecchi S, Isa F, Chrastina D, Isella G, Fedoryshyn Y, and Faist J, Phys. Rev. Lett. **109**, 057402 (2012).

[16] Xu C, Senaratne C L, Kouvetakis J, and Menéndez J, Appl. Phys. Lett. **105**, 232103, (2014).

[17] Shimura Y, Srinivasan S A, Van Thourhout D, Van Deun R, Pantouvaki M, Van Campenhout J and Loo R, Thin Solid Films 602, 56 (2016).

[18] Moriyama Y, Kamimuta Y, Kamata Y, Ikeda K, Sakai A, and Tezuka T, Appl. Phys. Express **7**, 2 (2014).

[19] Scappucci G, Capellini G, Lee W T C and Simmons M Y, Appl. Phys. Lett. **94**, 162106 (2009).

[20] Prucnal S et al, Sci. Rep. **6**, 27643 (2016)

[21] Milazzo R et al, J. Appl. Phys. **115**, 053501 (2014)

[22] Heo S, Baek S, Lee D, Hasan M, Jung H, Lee J, and Hwang H, Electrochem. Solid-State Lett. **9**, G136 (2006).

[23] Huang S H, Lu F L, Huang W L, Huang C H, and Liu C W, IEEE Electron Device Lett. **36**, 1114 (2015).

[24] Law S, Yu L, Rosenberg A and Wasserman D, *Nano Lett.* **13**, 4569 (2013)

[25] Wen H and Bellotti E, Phys. Rev. B **91**, 035307 (2015).

[26] Pizzi G, Virgilio M and Grosso G, Nanotechnology **21**, 55202 (2010).

[27] Isella G, Chrastina D, Rössner B, Hackbarth T, Herzog H J, König U, Von Känel H, Solid State Electron. **48**, 1317-1324 (2004)

[28] Millar R W, Gallacher K, Samarelli A, Frigerio J, Chrastina D, Isella G, Dieing T and Paul D J Optics Exp. **23**, 18193 (2015).

[29] Xu C, Senaratne C L, Kouvetakis J and Menéndez J, Phys. Rev. B **93**, 041201 (2016).

[30] Lockwood D J and Young J F, Light Scattering in Semiconductor Structures and Superlattices, eds. Springer (1991).

[31] Ref from Enrico

[32] Capellini G, De Seta M, Zaumseil P, Kozlowski G and Schroeder T, J. Appl. Phys. **111**, 73518 (2012).

[33] Grzybowski G, Roucka R, Mathews J, Jiang L, Beeler R, Kouvetakis J and Menéndez J, Phys. Rev. B 84, 205307 (2011).

[34] Wagner J, Solid. State. Electron. 28, 25 (1985).

[35] Camacho-Aguilera R, Han Z, Cai Y, Kimerling L C and Michel J, Appl. Phys. Lett. **102**, 152106 (2013).

[36] Jiang L, Gallagher J D, Senaratne C L, Aoki T, Mathews J, Kouvetakis J and Menéndez J, Semicond. Sci. Technol. 29, 115028 (2014)

[37] Xu C, Gallagher J D, Wallace P M, Senaratne C L, Sims P, Menéndez J. and Kouvetakis J, Semicond. Sci. Technol. 30, 105028 (2015)

[38] Teherani J, Chern W, Antoniadis D, Hoyt J, Ruiz L, Poweleit C and Menéndez J, Phys. Rev. B **85**, 205308 (2012).

[39] Ahmad C N and Adams A R, Phys. Rev. B **34**, 2319 (1986).

[40] Liu J, Cannon D, Wada K, Ishikawa Y, Danielson D, Jongthammanurak S, Michel J and Kimerling L, Phys. Rev. B **70**, 155309 (2004).